Biosensors and Bioelectronics 171 (2021) 112733

Contents lists available at ScienceDirect

Biosensors and Bioelectronics

journal homepage: http://www.elsevier.com/locate/bios

One-step quantification of salivary exosomes based on combined aptamer recognition and quantum dot signal amplification

Min Wu [a], Zhuokun Chen [a], Qihui Xie [a], Bolin Xiao [a], Gang Zhou [a,b], Gang Chen [a,c], Zhuan Bian [a,*]

[a] The State Key Laboratory Breeding Base of Basic Science of Stomatology (Hubei-MOST) and Key Laboratory of Oral Biomedicine Ministry of Education, School and Hospital of Stomatology, Wuhan University, Wuhan, 430079, PR China
[b] Department of Oral Medicine, School and Hospital of Stomatology, Wuhan University, Wuhan, 430079, PR China
[c] Department of Oral and Maxillofacial Surgery, School and Hospital of Stomatology, Wuhan University, Wuhan, 430079, PR China

ARTICLE INFO

Keywords:
Exosome
Aptamer
Quantum dot
Fluorescent biosensor

ABSTRACT

As promising fluid biomarkers for non-invasive diagnosis, naturally-occurring exosomes in saliva have attracted a wide interest for their potential application in oral diseases especially oral cancers. However, accurate quantification of salivary exosomes is still challenging due to the current difficulties in simultaneous identification and measurement of these nano-sized vesicles. In this study, we developed a novel fluorescent biosensor for one-step sensitive quantification of salivary exosomes based on magnetic and fluorescent bio-probes (MFBPs). Within the MFBPs, self-assembled DNA concatamers loaded with numerous quantum dots (QDs) were ingeniously tethered to aptamers, which were anchored on the surface of magnetic microspheres (MMs). Efficient recognition and capture of an exosome by the aptamer would simultaneously trigger the release of a DNA concatamer as the detection signal carrier, thereby generating a "one exosome-numerous QDs" amplification effect. As the result, this biosensor allowed one-step quantification with less assay time and achieved a high sensitivity with low limit of detection. Moreover, unique fluorescent properties of QDs and the superparamagnetism of MMs offered a strong anti-interference ability, enabling a robust quantification in complex matrices. Furthermore, this biosensor exhibited a good clinical feasibility with favorable accuracy comparable to nanoscale flow cytometry, and a superiority in label-free analysis and convenient operation. This study provides a novel and general strategy for one-step sensitive quantification of exosomes from body fluids, facilitating the development of exosome-based liquid biopsy for disease diagnosis.

1. Introduction

Exosomes are cell-derived nano-sized (30–150 nm) membrane vesicles that play critical roles in intercellular communication (Mathieu et al., 2019; van Niel et al., 2018; Colombo et al., 2014). In the past years, exosomes have been increasingly identified as diagnostic biomarkers due to their extensive presence in body fluids as well as their close association with disease development (Kalluri and LeBleu, 2020; Momen-Heravi et al., 2018). Saliva is one of the most versatile body fluids that contain naturally-occurring exosomes. As attractive fluid biomarkers for developing noninvasive diagnostics, salivary exosomes have recently gained significant attention for their potential application in oral diseases especially oral squamous cell carcinoma (OSCC) (Nair et al., 2018; Han et al., 2018; Xing et al., 2020). Recent studies have revealed that the level of salivary exosomes was significantly elevated in patients with OSCC, and the increased salivary exosomes showed close correlations with the malignant progression of OSCC, suggesting salivary exosomes as a promising biomarker for OSCC (Zhong et al., 2019; Zlotogorski-Hurvitz et al., 2016; Sharma et al., 2011). Therefore, a clinically feasible quantification technique for salivary exosomes could help to develop exosome-based liquid biopsy of OSCC.

Accurate quantification of exosomes, especially those from body fluids, is still challenging due to the current defects in simultaneous identification and measurement of these nano-sized vesicles. More complex than cell culture supernatants, body fluids comprise not only exosomes but also many non-exosomal components (e.g., protein aggregates, lipoproteins) that share similar physical properties to exosomes (Xu et al., 2016; Abramowicz et al., 2016). However, most of the commonly used methods to isolate exosomes from body fluids, including ultracentrifugation, ultrafiltration and size exclusion, are based on the

* Corresponding author.
E-mail address: bianzhuan@whu.edu.cn (Z. Bian).

https://doi.org/10.1016/j.bios.2020.112733
Received 11 August 2020; Received in revised form 7 October 2020; Accepted 13 October 2020
Available online 14 October 2020

physical properties of exosomes and cannot eliminate those non-exosomal contaminants from the isolated exosomes (Boriachek et al., 2018; Li et al., 2017). Thus, a specific function of exosome identification is of great importance to the techniques for accurately quantifying body fluid exosomes. But currently the major techniques for exosome quantification, which mainly rely on the measurement of total exosome proteins (e.g., BCA assay) or counting of individual exosome particles (e.g., nanoparticle tracking analysis, NTA), are unable to distinguish exosomes from non-exosomal contaminants (Shao et al., 2018). For quantification by BCA assay, exosomes have to be lysed to release the total proteins and then incubated with reaction regent containing Cu^{2+}, followed by the detection of changes in absorption spectra (Smith et al., 1985). However, the accuracy of this colorimetric assay, which aims at the total mass of proteins, is always restricted by the residue proteins mixed in the isolated exosomes from body fluids. In addition, this assay is relatively tedious and of limited sensitivity. As another commonly used technique, NTA employs a high-resolution camera to capture and record the scattered light of individual particle under Brownian motion, allowing simultaneous determination of the size distribution and particle concentration. However, when applied to quantify exosomes from body fluids, NTA often provide inaccurate concentration information owing to the interference from protein aggregates and lipoprotein particles (Kim et al., 2019).

For better identification of exosomes before quantification, several affinity-based techniques, such as enzyme-linked immunosorbent assay (ELISA), nanoscale flow cytometry (NanoFCM), have been utilized to quantify exosomes from body fluids via selective recognition and binding of exosomal markers (Shao et al., 2018; Cheng et al., 2019). ELISA is a heterogeneous reaction with slow binding kinetics on solid-liquid interface. With the specific "sandwich" configuration, ELISA enables the specific quantification of exosomes by using capture antibodies against CD63, a marker tetraspanin enriched on exosomes (Kowal et al., 2016). But the drawbacks of ELISA in time-consuming and tedious operation make it unsuitable for clinical implementation (Huang et al., 2020a). The recent emergence of NanoFCM, capable of detecting nano-sized particles, provides a powerful tool for precise quantification and phenotyping of exosomes (Tian et al., 2020; Choi et al., 2019). However, its clinical application is held back by the customized equipment and specialized operation. Moreover, prior to the detection with NanoFCM, exosomes have to be pre-labeled by fluorescent antibodies and then washed repeatedly to remove the excess antibodies, resulting in tedious operations and inconveniences of downstream exosome analysis. Therefore, the affinity-based quantification strategies for exosomes from body fluids still need to be improved for a better performance.

The recognition element is of critical importance to the performance of affinity-based quantification techniques (Cheng et al., 2019). Aptamers, short single-stranded oligonucleotides with unique tertiary structures, are appealing recognition element for specific binding to the interested targets (Kim et al., 2016; Ma et al., 2015; Wang et al., 2019). In comparison with antibodies, aptamers are superior in easy synthesis, facile modification, low cost, and high stability in body fluids (Wu et al., 2020). Moreover, aptamers have unique properties of small size (2–3 nm), favorable affinity and good specificity, making them as ideal recognition ligands to exosomes (Zhu et al., 2020a; Liu et al., 2019). One of the most widely employed aptamers in exosome analyses is the aptamer against exosomal marker CD63 (Wu et al., 2020). Moreover, the high programmability and flexibility of aptamers permit various strategies for signal amplification in exosome detecting (Meng et al., 2016). Such merits of aptamers have promoted the development of various affinity-based sensing platforms for exosome quantification, including electrochemistry (Cao et al., 2019; Zhang et al., 2019a; Dong et al., 2018; Wang et al., 2017; Huang et al., 2019), colorimetry (Jiang et al., 2017; Zhang et al., 2019d; Xia et al., 2017), fluorometry (Zhang et al., 2019e; Jin et al., 2018; Huang et al., 2020b), surface-enhanced raman scattering (Zhang et al., 2019c; Wang et al., 2018), and giant magnetoresistance (Zhu et al., 2020b). For example, Cao and colleagues developed a catalytic molecule machine-driven electrochemical biosensor for detection of HepG2 cell-derived exosomes (Cao et al., 2019). By utilizing DNA-capped single-walled carbon nanotubes, Xia and colleagues achieved the convenient colorimetric exosome detection with a limit of detection of 5.2×10^5 particles/μL (Xia et al., 2017). Based on the affinity between aptamers and membrane proteins on exosomes, Zhang and colleagues proposed a fluorescence polarization assay for quantification of exosomes in the plasma from lung cancer patients (Zhang et al., 2019e).

In this work, we proposed a novel fluorescent biosensor for convenient, sensitive and label-free quantification of salivary exosomes based on magnetic and fluorescent bio-probes (MFBPs), which were ingeniously and controllably constructed by integrating aptamers, magnetic microspheres (MMs), DNA concatamers and quantum dots (QDs) (Scheme 1A). Aptamers, anchored on the surface of MMs and tethered to DNA concatamers, were employed to recognize and bind CD63 proteins on exosomes. The conformational switch of aptamers triggered by aptamer-exosome interaction would cause the release of DNA concatamers. These long DNA concatamers were engineered by the self-assembly of DNA growth and were conjugated with numerous QDs via the strong interaction between biotin and streptavidin. As the carrier of detection signal, the QD-loaded DNA concatamer can greatly amplify the detection signal upon the capture of an exosome by the aptamer, thus generating a "one exosome-numerous QDs" amplification effect. The exosome quantification biosensor developed in this study exhibited a high sensitivity with low limit of detection, the convenience of one-step operation without pre-labeling, strong anti-interference ability in complex matrices, and clinical feasibility with favorable accuracy, thereby possessing great potential for future applications.

2. Materials and methods

2.1. Preparation of MMs-Apt

The CD63 aptamers (Apt_{CD63}) were dissolved in distilled deionized water and heated to 95 °C for 10 min, followed by cooling at 4 °C. 1 mg of MMs was suspended in 200 μL of phosphate buffer (0.01 M, pH 7.2). Subsequently, 4 mg of EDC was immediately dissolved in 200 μL of phosphate buffer, followed by addition EDC solution and 2 μL of 1 μM Apt_{CD63} to the MMs suspension. After incubation for 4 h at 25 °C with a gentle shaking, the resulting MMs-Apt were washed with phosphate buffer by magnetic separation to remove excess Apt_{CD63}.

2.2. Construction and characterization of MFBPs

Firstly, 1 mg of MMs-Apt was resuspended in 200 μL of binding buffer (10 mM HEPES, 1 M NaCl, 50 mM $MgCl_2$, pH 7.2). Secondly, 2 μL of 10 μM biotin-modified reporting DNA 1 (R1) and reporting DNA 2 (R2) were added into MMs-Apt suspension. After incubation for 1 h at 25 °C with a gentle shaking, the MMs-Apt-$(R1\text{-}R2)_n$ were washed to remove excess R1 and R2. Thirdly, 10 μL of 1 μM streptavidin-conjugated QDs (SA-QDs) were incubated with MMs-Apt-$(R1\text{-}R2)_n$ for 1 h at 25 °C with a gentle shaking. Finally, the resulting MFBPs were washed with binding buffer to remove excess SA-QDs, then stored at 4 °C for further use. The sequences of Apt_{CD63}, R1 and R2 are listed in Table S1. The self-assembly of DNA concatamers was examined by 15% polyacrylamide gel electrophoresis (PAGE) gel staining with GelRed.

2.3. Generation and characterization of exosomes

Human oral squamous cell carcinoma CAL27 cells were grown in high-glucose DMEM medium contained 10% exosome-free FBS and 1% antibiotics. CAL27 cell-derived exosomes were collected by ultracentrifugation from cell culture supernatant. Briefly, the collected cell culture supernatant was centrifuged at 2000 g for 20 min to remove cell

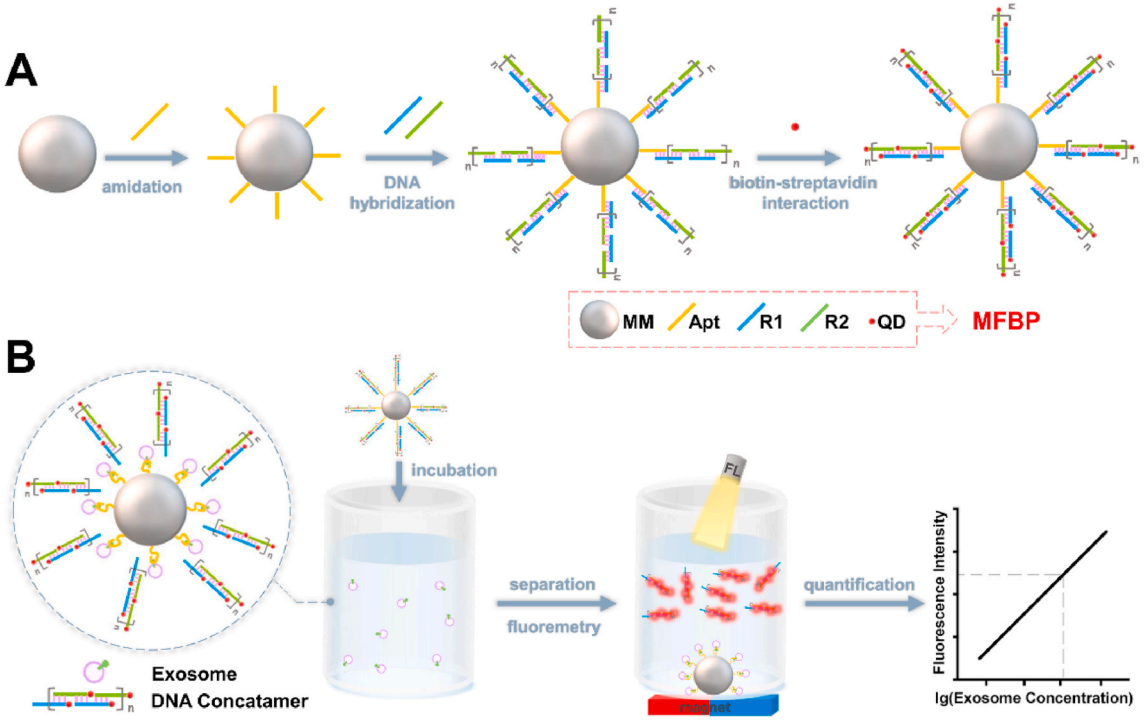

Scheme 1. (A) Schematic illustration of MFBP constructing process. (B) Sensing principle of MFBP-based one-step quantification of exosomes.

debris and apoptotic bodies. After centrifugation at 20,500 g for 60 min to remove microvesicles, the supernatant was ultracentrifuged at 120,000 g for 70 min to obtain exosome pellet. Subsequently, the pellet was washed with PBS by ultracentrifugation at 120,000 g for 70 min. Then the purified exosomes was obtained by suspending final pellet with PBS. After negative staining with phosphotungstic acid for 3 min at 25 °C, the morphology of exosomes was observed by transmission electron microscope (TEM). Western blotting analysis was used to verify exosomal protein expression using CD63, HRS primary antibody. NanoFCM analysis was used to assess the binding efficiency of exosomes by Apt_{CD63}.

2.4. Quantification of exosomes

The exosomes were incubated with MFBPs in binding buffer with a final volume of 200 μL. After incubation for 30 min at 25 °C with a gentle shaking, the resulting MFBP-exosome complexes were separated by a magnetic scaffold. The supernatant containing detection signal carries was measured by a fluorescence spectrometer. The fluorescence images of MFBPs before and after the incubation with CellMask Deep Red-stained exosomes were recorded with a fluorescence microscope.

2.5. Analysis of salivary exosomes

The human saliva samples from healthy donors and patients with OSCC were obtained from Hospital of Stomatology, Wuhan University. This work was carried out according to the guidelines approved by the ethics committees from the institutions involved. The clinical information of patients was presented in Table S2. Human saliva was collected into sterile tubes and immediately centrifuged twice at 2600 g for 10 min at 4 °C. After centrifugation at 20,500 g for 60 min, salivary exosomes was obtained by ultracentrifugation at 120,000 g for 70 min. Salivary exosomes were diluted with definite ratio and were incubated with MFBPs in binding buffer. The following quantification steps are described above. NTA and NanoFCM was employed to quantify the salivary exosomes.

3. Results and discussion

3.1. Construction and characterization of MFBPs

The MMs, which had a polystyrene microsphere core/Fe_3O_4 nanoparticles magnetic layer/silica outer shell structure, showed the characteristics of uniform size distribution, excellent superparamagnetic property, and high biomolecule coupling efficiency. The fluorescence microscopy image showed that the monodispersed MMs were efficiently modified with Apt_{CD63} (Fig. 1A). The flow cytometry result further confirmed that the coupling efficiency of Apt_{CD63} to MMs reached up to 98.1% (Fig. 1B). Successful self-assembly of DNA concatamer was verified by native polyacrylamide gel electrophoresis (Fig. 1C). As shown in Lane 6, the long DNA concatamers were created through consecutive DNA hybridization between R1 and R2. Meanwhile, the self-assembly of DNA concatamers was not affected in the presence of Apt_{CD63} at M ratio of 1:50:50 (Apt_{CD63}: R1: R2) (Lane 7) and SA-QDs (Lane 8). With the aid of the hybridization between R1 and Apt_{CD63}, the long DNA concatamers were successfully self-assembled on MMs-Apt, as proved by the significantly increased hydrodynamic diameter of MMs-Apt-(R1-R2)n (Fig. 1D). In virtue of the specific and strong interaction between biotin and streptavidin (Kd ~10^{-14} M) (Dundas et al., 2013), biotin-modified DNA concatamers could bind numerous SA-QDs to form MFBPs, leading to a further increased hydrodynamic diameter (Fig. 1D) and the changed zeta potential (Fig. S1). The SA-QDs used here were streptavidin-conjugated ZnCdSe/ZnS core/shell QDs, exhibiting small and uniform size, narrow full width at half maximum (30 nm), maximum excitation wavelength at 393 nm, and maximum emission wavelength at 605 nm (Fig. S2). It was revealed that the fluorescent intensity of MFBPs was much more stronger than that without DNA concatamers (MMs-Apt-R1-QD), demonstrating a good fluorescence enhancement endowed by the long DNA concatamers loaded with a large amount of QDs (Fig. 1E). Consistently, MFBPs displayed significantly stronger fluorescence signals than MMs-Apt-R1-QD, while no fluorescence signal was observed in MMs and MMs-Apt after incubation with SA-QDs (Fig. 1F), indicating little non-specific adsorption of SA-QDs to MMs and MMs-Apt. The narrow distribution of

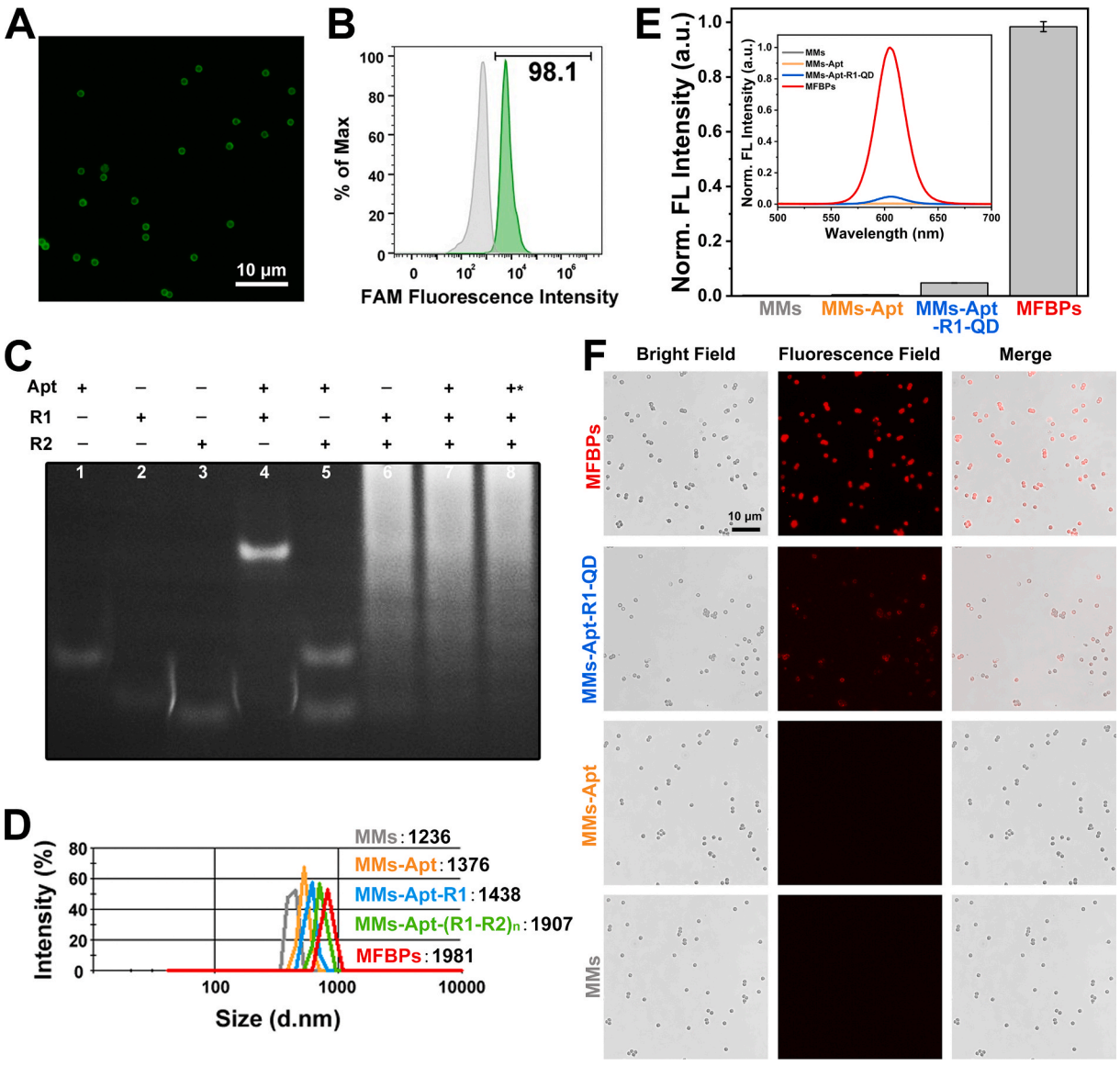

Fig. 1. (A) Fluorescence microscopic image of MMs after modifying with FAM-labeled Apt_{CD63}. (B) Flow cytometry analysis of MMs-Apt. (C) Native PAGE verified the self-assembly of DNA concatamers (Lane 1: Apt_{CD63} (1 μM), Lane 2: R1 (1 μM), Lane 3: R2 (1 μM), Lane 4: Apt_{CD63} and R1 (1 μM each), Lane 5: Apt_{CD63} and R2 (1 μM each), Lane 6: R1 and R2 (1 μM each), Lane 7: Apt_{CD63} (20 nM), R1 and R2 (1 μM each), Lane 8: Apt_{CD63} (20 nM), SA-QDs (2 μM), R1 and R2 (1 μM each)). (D) Hydrodynamic diameters of MMs, MMs-Apt, MMs-Apt-R1, MMs-Apt-$(R1-R2)_n$, and MFBPs. (E) Fluorescence intensities and fluorescence spectrums (Inset) of MMs, MMs-Apt, MMs-Apt-R1-QD, and MFBPs (a.u.: arbitrary unit). (F) Fluorescence microscopic images of MFBPs, MMs-Apt-R1-QD, MMs-Apt and MMs after incubation with SA-QDs (Fluorescence Field: excitation 561 nm, emission 605/20 nm, Merge: merge of bright and fluorescence filed).

fluorescence intensity as shown by flow cytometry suggested the fluorescence uniformity of MFBPs (Fig. S3). To test the stability of MFBPs, the hydrodynamic diameter and zeta potential of newly-prepared MFBPs were compared with those after 14 days' storage. The results suggested negligible difference between them (Table S3). In addition, the fluorescence intensity of MFBPs remained unchanged after 14 days' storage (Fig. S4), confirming the favorable stability of MFBPs.

3.2. Characterization of exosomes

Human oral squamous cell carcinoma CAL27 cell derived-exosomes, as the model exosomes in this work, were purified from the cell culture supernatant by ultracentrifugation. As detected by NTA, the particle concentration and average hydrodynamic diameter of exosomes was 3.5×10^{12} particles/mL and 131 nm, respectively (Fig. 2A). The TEM image showed the characteristic morphology of exosomes, which were membrane vesicles surrounded by a lipid bilayer (Fig. 2B). Moreover, an obvious band of exosomal CD63 was observed from western blotting (Fig. 2C), confirming the abundance of CD63 on exosomes. Additionally, the results of NanoFCM revealed that approximate 88.1% of the exosomes were successfully recognized and bound by Apt_{CD63}, demonstrating the high expression of CD63 as well as the good binding efficiency of Apt_{CD63} to the exosomes (Fig. 2D). Therefore, it is feasible to utilize Apt_{CD63} to recognize and bind exosomes in this work.

3.3. Efficient capture of exosomes and simultaneous release of DNA concatamers

The results from NTA showed that there was a significantly decrease in the exosome concentration after incubation with MMs-Apt, while little change was observed after incubation with MMs alone or MMs functionalized with random DNA library (MMs-Lib), indicating the high efficiency of MMs-Apt in capturing exosomes (Fig. 3A). As evidenced by TEM, many exosomes with intact morphology were bound to MMs-Apt

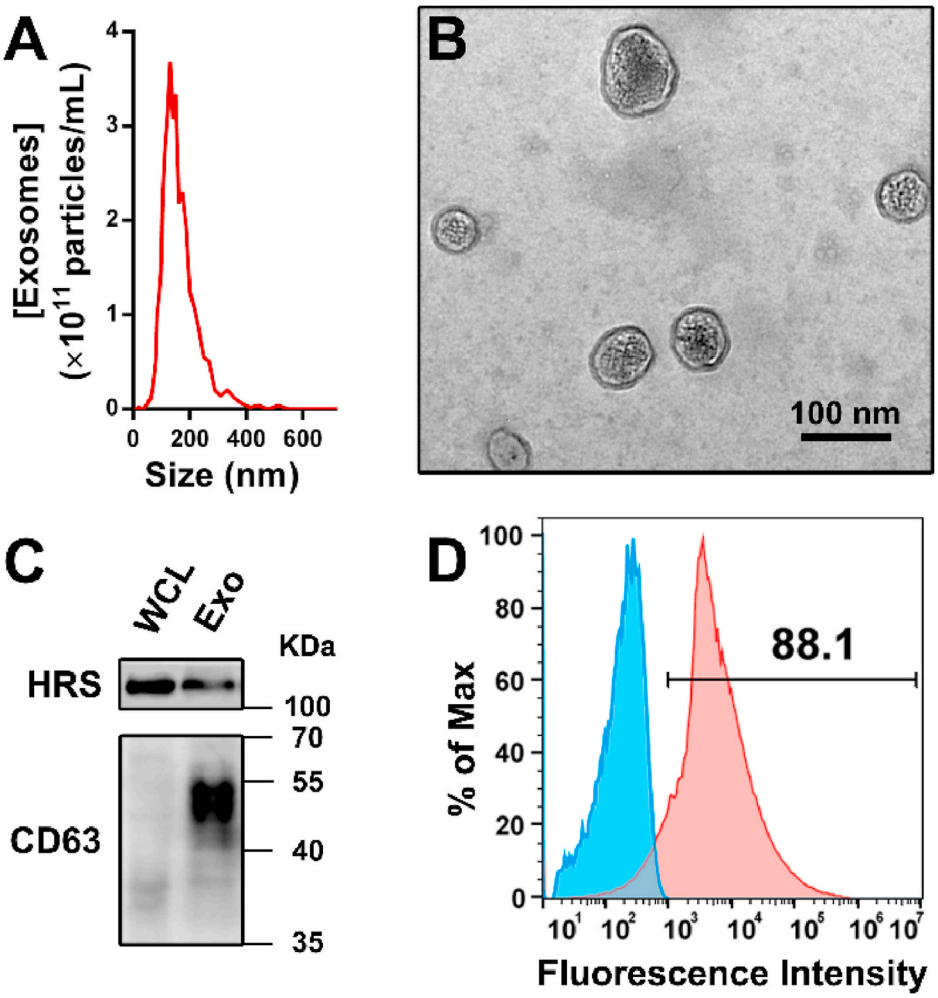

Fig. 2. NTA (A) and TEM image (B) of purified exosomes. (C) Western blotting analysis of HRS and CD63 expression on whole cell lysis (WCL) and exosomes (Exo). (D) The binding efficiency of Apt_{CD63} to exosomes analyzed by NanoFCM.

(Fig. 3B), demonstrating the specific and effective binding between MMs-Apt and exosomes. To investigate the ability of MFBPs to capture exosomes, the concentrations of exosomes left in supernatant after treatment with different functionalized MMs were examined. As shown in Fig. 3C, compared with MMs or MMs-Lib, both MFBPs and MMs-Apt exhibited a good ability to capture exosomes. The capture efficiencies between MFBPs and MMs-Apt showed no significant difference, implying that the aptamer-based recognition of exosomes was not affected by the DNA concatamers tethered to aptamers.

To investigate whether MFBPs can simultaneously release DNA concatamers upon the capture of exosomes, the fluorescence images of MFBPs were taken before and after the incubation with exosomes (Fig. 3D). It was revealed that the green signals of aptamers colocalized well with the blue signals of exosomes, confirming the efficient recognition and capture of exosomes by MFBPs (Fig. 3E, Left). Additionally, the line profile of the distribution and intensity of aptamers (green) and exosomes (blue) on the white line also proved the efficient binding between MFBPs and exosomes (Fig. 3E, Right). To verify the release of DNA concatamer upon exosome capture, the colocalization efficiency between aptamers and DNA concatamers were compared before and after the incubation with exosomes. As shown in Fig. 3D, compared with pre-incubation group, less red singles of DNA concatamers but unchanged green singles of aptamers were observed in the presence of exosomes, indicating that the exosome-aptamer interaction would cause the release of DNA concatamers. Moreover, the values of Manders coefficient of green signals in thresholded image (tMg) and the intensity correlation quotient (ICQ) were significantly reduced after incubation with exosomes (Fig. 3F), suggesting that the percentage of green signals colocalized with red signals was dropping (Bolte and Cordelieres, 2006). This result further confirmed the release of DNA concatamers upon exosome capture, which is possibly due to the conformational switch of aptamers triggered by aptamer-exosome interaction. Therefore, it is concluded that MFBPs can efficiently capture exosomes and simultaneously release uniform DNA concatamers as detection signal carriers, establishing a sound basis for exosome quantification.

3.4. Condition optimization, sensitivity and repeatability

As described in Scheme 1B, a novel fluorescent biosensor for one-step quantification of exosome was developed by using MFBPs. By incubation of the exosomes with MFBPs in binding buffer, the capture of exosomes and the release of DNA concatamers carrying numerous QDs could be synchronously achieved. After magnetic separation of the MFBP-exosome complexes, the fluorescence intensity of released DNA concatamers in the supernatant was measured. To achieve the best performance in exosome quantification, the dosage of MFBPs and the incubation time of MFBPs with exosomes were optimized. As shown in Fig. S5, 0.25 mg/mL of MFBPs and 0.5 h of incubation time were confirmed as the optimal experimental conditions. In comparison with most of the currently reported approaches for exosome quantification, our one-step method significantly simplified the detection process and shortened the assay time (Table S4). Fig. 4A displays the three-

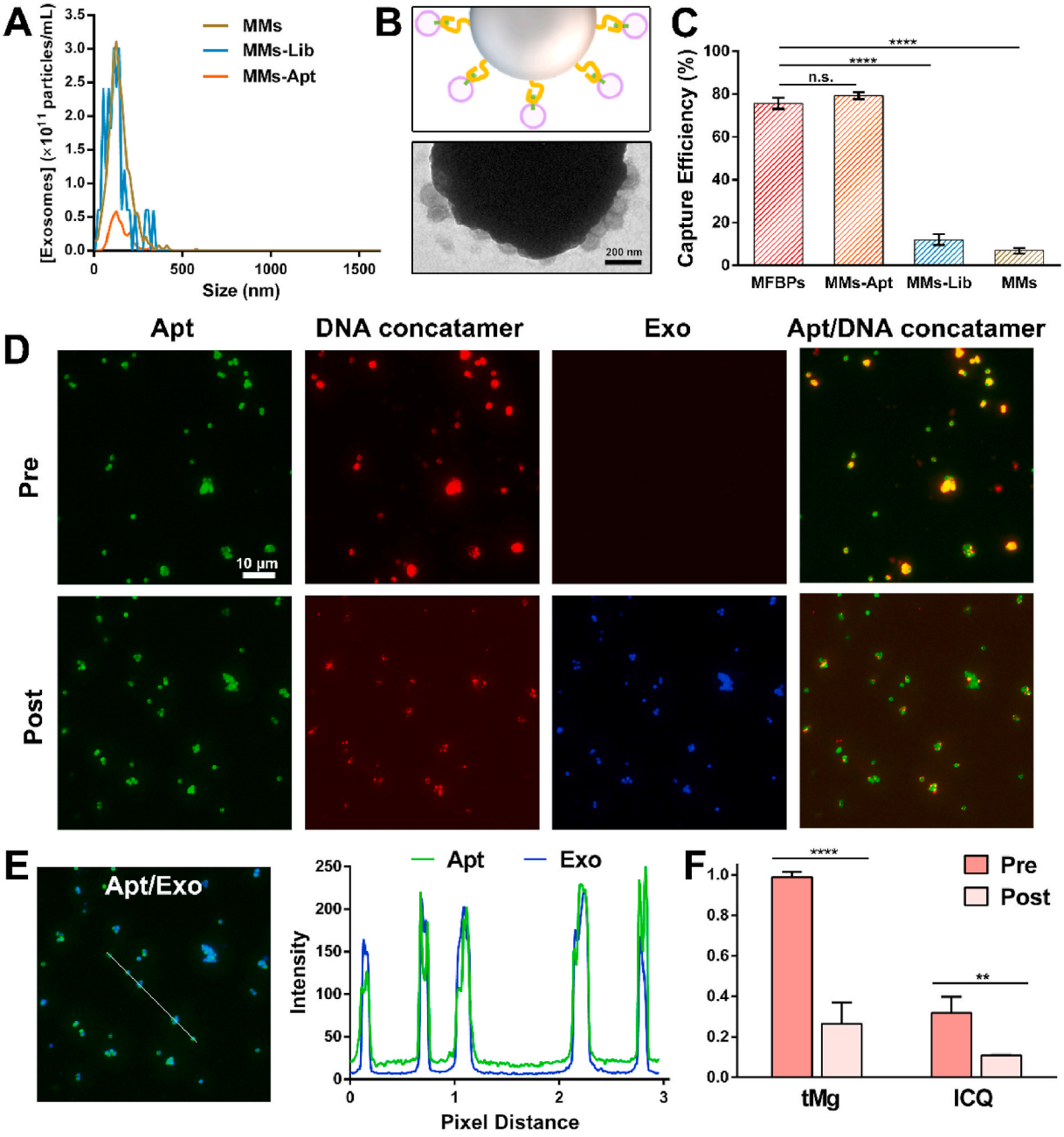

Fig. 3. (A) Quantification exosomes left in supernatant after treatment with MMs, MMs-Lib and MMs-Apt by NTA. (B) Schematic (Top) and TEM image (Bottom) of capturing exosomes by MMs-Apt. (C) Capture efficiencies of MFBPs, MMs-Apt, MMs-Lib and MMs to exosomes (one-way ANOVA: n. s. not significant ($P > 0.05$), ****$P < 0.0001$, n = 3). (D) Fluorescence microscopic images of MFBPs before and after the incubation with exosomes (FAM-labeled Apt_{CD63} (green), QDs-bound DNA concatamers (red), CellMask Deep Red-stained exosomes (pseudo-colored blue), and merge images of green and red signals). (E) Colocalization analysis of aptamers and exosomes (Left: merge image of green and blue signals from post-incubation group, Right: line profile of the distribution and intensity of aptamers and exosomes on the white line). (F) Colocalization efficiencies between aptamers and DNA concatamers before and after the incubation with exosomes (*t*-test: ****$P < 0.0001$, **$P < 0.01$, n > 3). (For interpretation of the references to color in this figure legend, the reader is referred to the Web version of this article.)

dimensional fluorescence spectra of detecting exosomes in the range of 500 to 10^5 particles/μL. The fluorescence intensities at 605 nm gradually enhanced with the increasing concentrations of exosomes (Fig. 4B). Linear regression analysis of fluorescence intensities versus logarithm of the exosome concentrations resulted in a coefficient of determination (R^2) value of 0.998 (Fig. 4C), indicating a strong linear relationship between the detected fluorescence intensities and the logarithmic concentrations of exosomes. This result confirmed that our proposed fluorescent biosensor had a good capacity in exosome quantification. As shown in Fig. 4D, the detected fluorescence signal using MFBPs was approximately 14-flod higher than that without the DNA concatamers. This is because the long DNA concatamers loaded with a large amount of QDs can greatly amplify the detection signal, generating a "one exosome-numerous QDs" amplification effect. Therefore, our proposed biosensor for one-step quantification of exosome exhibited high sensitivity with low limit of detection (500 particles/μL), wide detection range (three orders of magnitude), and good quantitative capacity (R^2 = 0.998). The sensitivity of our proposed biosensor, which was comparable to or better than most of the currently reported exosome sensing platforms, could fully satisfy the requirements of clinical quantitative detection (Table S4). Additionally, the intra-assay and inter-assay variabilities of this biosensor were determined as 3.09% and 5.43%,

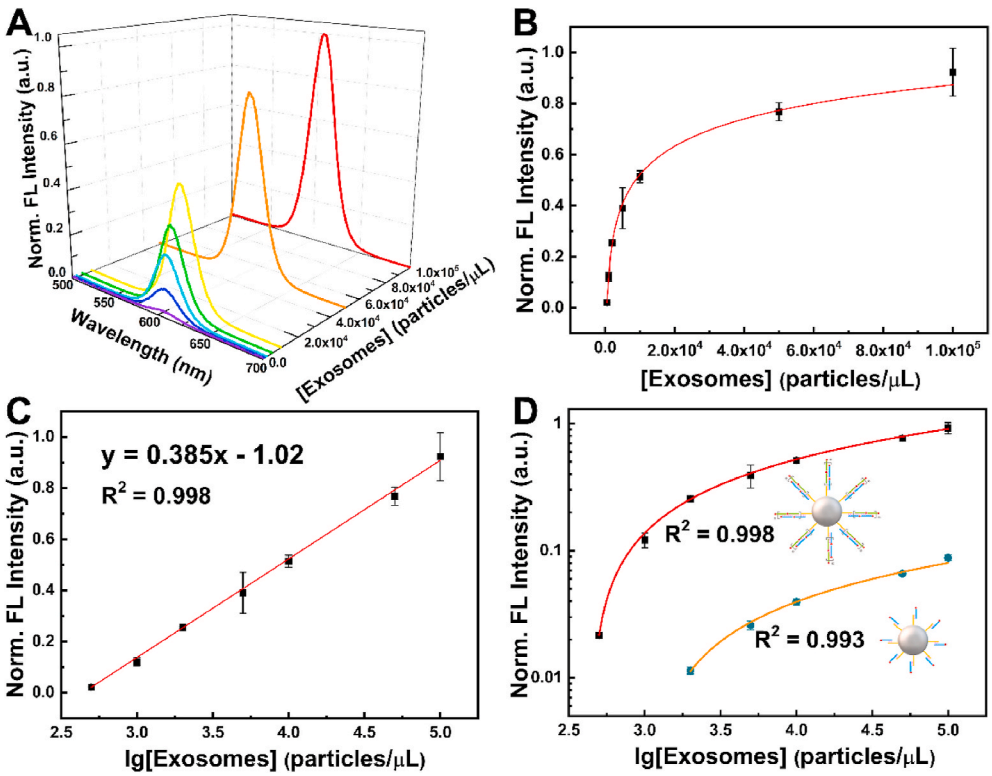

Fig. 4. (A) Three-dimensional fluorescence spectra of detecting exosomes at different concentrations (500 - 10^5 particles/μL). (B) Calibration plots of fluorescence intensities versus exosome concentrations. (C) Linear relationship of fluorescence intensities versus logarithm of the exosome concentrations. The units of the intercept and slope in the calibration are arbitrary unit (a.u.) and a. u./lg (particles/μL), respectively; R^2 represents the proportion of the variance in the dependent variable (fluorescence intensity, here) that is predictable from the independent variable (logarithm of the exosome concentration, here). The range of the R^2 value lies between 0 and 1, which gives information about the goodness of fit for linear models ($R^2 = 0$, no correlation at all; $R^2 = 1$, perfect linear relationship). (D) Calibration plots of fluorescence intensities versus logarithm of the exosome concentrations using MFBPs (red line) and MMs-Apt-R1-QD (orange line). (n = 3). (For interpretation of the references to color in this figure legend, the reader is referred to the Web version of this article.)

respectively (Table S5), suggesting the good repeatability of this MFBP-based exosome quantification biosensor.

3.5. Anti-interference ability in complex matrices

To examine the anti-interference ability of our proposed biosensor, it was employed to detect spiked exosomes in different complex matrices. Human saliva, whose intrinsic exosomes were pre-excluded by ultracentrifugation, were mixed with the binding buffer at different volume ratios to mimic the complex matrices. As shown in Fig. 5A, the resulting fluorescence intensities in 25%, 50% and 75% v/v saliva were similar to those in binding buffer alone, suggesting that this biosensor was feasible to detect exosomes in complex matrices. Then, we assess the quantitative ability of this biosensor to detect spiked exosomes in different matrices, including binding buffer alone, binding buffer containing polystyrene nanospheres (PS-NPs), exosome-excluded human saliva, and exosome-excluded human saliva containing PS-NPs (Fig. 5B). The statistical analysis result showed that the quantitative capacities of our proposed biosensor in these different matrices were comparable and had no significant difference (Table S6), indicating its strong anti-interference ability in complex matrices. Of note, even in the presence of non-exosomal contaminants (PS-NPs) at a high concentration, the MFBP-based biosensor can be well applied to quantify the spiked exosomes. This is probably due to the fact that, unlike the biochemical property- or physical property-based quantification methods, this biosensor utilizes the efficient and specific interaction between the aptamers and exosomes, thereby being capable to reflect the accurate concentration of exosomes without the interference from non-exosomal contaminants. Additionally, it is worth mentioning that QDs have unique fluorescent properties of outstanding brightness, large Stokes shift and photostability, allowing stable detection signals in complex matrices (Zhang et al., 2019b). Meanwhile, the good superparamagnetism of MMs enables the removal of interference signal with convenient manipulation. Such merits facilitate a strong

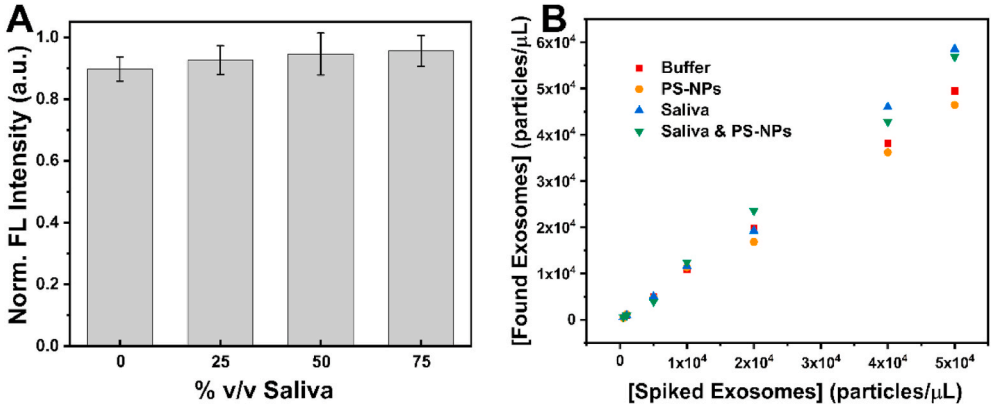

Fig. 5. (A) Fluorescence intensities of detecting spiked exosomes (10^4 particles/μL) in binding buffer alone (0%), and exosome-excluded 25%, 50% and 75% v/v saliva. (B) Quantitative capacities to detect spiked exosomes at different concentrations (500–5 × 10^4 particles/μL) in four types of matrices: Binding buffer (■), Binding buffer containing PS-NPs (100 nm, 8 × 10^4 particles/μL) (●), Exosome-excluded human saliva (50% v/v) (▲), Exosome-excluded human saliva (50% v/v) containing PS-NPs (100 nm, 8 × 10^4 particles/μL) (▼).

anti-interference ability of our proposed biosensor in complex matrices.

3.6. Clinical feasibility

To further test the clinical feasibility of our proposed biosensor, we compare it with NTA and NanoFCM by quantifying salivary exosomes isolated from healthy donors and patients with OSCC (Fig. S6). As shown in Fig. 6, the detected concentrations of salivary exosomes were comparable between NanoFCM and this biosensor, while higher concentrations were obtained by NTA. This is possibly due to that the non-exosomal contaminations (e.g., protein aggregates and lipoproteins), which inevitably entrained in salivary exosomes, were also quantified by NTA. Although showing similar affinity-based principle and quantification accuracy to NanoFCM, our proposed biosensor was still superior to NanoFCM in terms of no need to pre-label exosomes with fluorescent antibodies against CD63. The above results verified that our proposed biosensor exhibited a good clinical feasibility to identify and quantify human salivary exosomes. By using CD63 as the model protein, the present study aims to develop a general and one-step sensitive strategy to detect the level of exosomal proteins, so as to quantify the exosome concentrations. It could be prospected that quantifying the level of some cancer-specific exosomal proteins, e.g. our previously reported exosomal PD-L1 (Chen et al., 2018), will provide a better clinical value. In the future, by further modification with different specific aptamers, this biosensor would facilitate the one-step quantification of different exosome sub-populations that carry cancer-specific proteins, providing a higher diagnostic accuracy into salivary exosome-based liquid biopsy.

4. Conclusions

In summary, a convenient, sensitive and label-free biosensor for quantifying body fluid exosomes was established in the present study by utilizing MFBPs, which ingeniously integrated aptamers, MMs, DNA concatamers and QDs. This MFBP-based fluorescent biosensor possesses several advantages. First, MFBPs were able to efficiently capture exosomes and simultaneously release the QD-loaded DNA concatamers, enabling one-step quantification with convenient operation. Second, DNA concatamers loaded with a large amount of QDs could generate the “one exosome-numerous QDs” signal amplification effect, offering a high sensitivity with low limit of detection. Third, the good superparamagnetism of MMs and unique fluorescent properties of QDs provided a strong anti-interference ability in complex matrices, allowing a robust exosome quantification in human saliva. Fourth, compared to scatter light-dependent NTA, our proposed biosensor was based on specific aptamer-exosome interaction and could provide accurate exosome concentrations without the interference from non-exosomal contaminants. Last but not least, this biosensor was validated with clinical salivary samples, resulting in a consistence with NanoFCM, and displayed the superiority in label-free analysis. Given the above advantages, we speculate that the present work could provide new insights into salivary exosome-based liquid biopsy. Moreover, by further modification with different specific aptamers, this work would facilitate the characterization and quantification of cancer-specific sub-populations of exosomes from various body fluids, which is of importance for giving diagnostic information with a higher accuracy.

CRediT authorship contribution statement

Min Wu: Conceptualization, Methodology, Investigation, Formal analysis, Validation, Funding acquisition, Writing - original draft. **Zhuokun Chen:** Investigation, Formal analysis. **Qihui Xie:** Investigation, Formal analysis. **Bolin Xiao:** Investigation, Formal analysis, Validation. **Gang Zhou:** Resources, Writing - review & editing. **Gang Chen:** Conceptualization, Resources, Writing - review & editing. **Zhuan Bian:** Supervision, Funding acquisition, Project administration, Writing - review & editing.

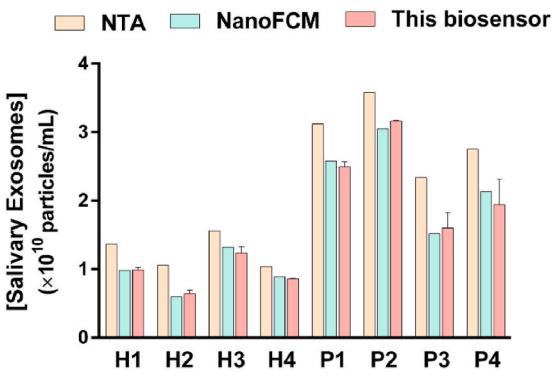

Fig. 6. Comparison of this biosensor with NTA and NanoFCM for quantifying salivary exosomes from healthy donors (H) and OSCC patients (P).

Declaration of competing interest

The authors declare that they have no known competing financial interests or personal relationships that could have appeared to influence the work reported in this paper.

Acknowledgments

We gratefully appreciate the financial support from the National Natural Science Foundation of China (81901887, 81970923), the National Key Research and Development Program of China (2016YFC1000505), the Key Research Program of the Provincial Department of Science and Technology (No. 2017ACA181), and the Fundamental Research Funds for the Central Universities (2042020kf0183).

Appendix A. Supplementary data

Supplementary data to this article can be found online at https://doi.org/10.1016/j.bios.2020.112733.

References

Abramowicz, A., Widlak, P., Pietrowska, M., 2016. Proteomic analysis of exosomal cargo: the challenge of high purity vesicle isolation. Mol. Biosyst. 12 (5), 1407–1419.
Bolte, S., Cordelieres, F.P., 2006. A guided tour into subcellular colocalization analysis in light microscopy. J. Microsc. 224, 213–232.
Boriachek, K., Islam, M.N., Moller, A., Salomon, C., Nguyen, N.T., Hossain, M.S.A., Yamauchi, Y., Shiddiky, M.J.A., 2018. Biological functions and current advances in isolation and detection strategies for exosome nanovesicles. Small 14 (6), 1702153.
Cao, Y., Li, L., Han, B., Wang, Y., Dai, Y., Zhao, J., 2019. A catalytic molecule machine-driven biosensing method for amplified electrochemical detection of exosomes. Biosens. Bioelectron. 141, 111397.
Chen, G., Huang, A.C., Zhang, W., Zhang, G., Wu, M., Xu, W., Yu, Z., Yang, J., Wang, B., Sun, H., Xia, H., Man, Q., Zhong, W., Antelo, L.F., Wu, B., Xiong, X., Liu, X., Guan, L., Li, T., Liu, S., Yang, R., Lu, Y., Dong, L., McGettigan, S., Somasundaram, R., Radhakrishnan, R., Mills, G., Lu, Y., Kim, J., Chen, Y.H., Dong, H., Zhao, Y., Karakousis, G.C., Mitchell, T.C., Schuchter, L.M., Herlyn, M., Wherry, E.J., Xu, X., Guo, W., 2018. Exosomal PD-L1 contributes to immunosuppression and is associated with anti-PD-1 response. Nature 560 (7718), 382–386.
Cheng, N., Du, D., Wang, X., Liu, D., Xu, W., Luo, Y., Lin, Y., 2019. Recent advances in biosensors for detecting cancer-derived exosomes. Trends Biotechnol. 37 (11), 1236–1254.
Choi, D., Montermini, L., Jeong, H., Sharma, S., Meehan, B., Rak, J., 2019. Mapping subpopulations of cancer cell-derived extracellular vesicles and particles by nano-flow cytometry. ACS Nano 13 (9), 10499–10511.
Colombo, M., Raposo, G., Thery, C., 2014. Biogenesis, secretion, and intercellular interactions of exosomes and other extracellular vesicles. Annu. Rev. Cell Dev. Biol. 30, 255–289.
Dong, H., Chen, H., Jiang, J., Zhang, H., Cai, C., Shen, Q., 2018. Highly sensitive electrochemical detection of tumor exosomes based on aptamer recognition-induced multi-DNA Release and cyclic enzymatic amplification. Anal. Chem. 90 (7), 4507–4513.
Dundas, C.M., Demonte, D., Park, S., 2013. Streptavidin-biotin technology: improvements and innovations in chemical and biological applications. Appl. Microbiol. Biotechnol. 97 (21), 9343–9353.

Han, Y., Jia, L., Zheng, Y., Li, W., 2018. Salivary exosomes: emerging roles in systemic disease. Int. J. Biol. Sci. 14 (6), 633–643.
Huang, M., Yang, J., Wang, T., Song, J., Xia, J., Wu, L., Wang, W., Wu, Q., Zhu, Z., Song, Y., Yang, C., 2020a. Homogeneous, low-volume, efficient, and sensitive quantitation of circulating exosomal PD-L1 for cancer diagnosis and immunotherapy response prediction. Angew. Chem., Int. Ed. Engl. 59 (12), 4800–4805.
Huang, R.R., He, L., Li, S., Liu, H.N., Jin, L., Chen, Z., Zhao, Y.X., Li, Z.Y., Deng, Y., He, N. Y., 2020b. A simple fluorescence aptasensor for gastric cancer exosome detection based on branched rolling circle amplification. Nanoscale 12 (4), 2445–2451.
Huang, R., He, L., Xia, Y., Xu, H., Liu, C., Xie, H., Wang, S., Peng, L., Liu, Y., Liu, Y., He, N., Li, Z., 2019. A sensitive aptasensor based on a hemin/G-quadruplex-assisted signal amplification strategy for electrochemical detection of gastric cancer exosomes. Small 15 (19), 1900735.
Jiang, Y., Shi, M., Liu, Y., Wan, S., Cui, C., Zhang, L., Tan, W., 2017. Aptamer/AuNP biosensor for colorimetric profiling of exosomal proteins. Angew. Chem., Int. Ed. Engl. 56 (39), 11916–11920.
Jin, D., Yang, F., Zhang, Y., Liu, L., Zhou, Y., Wang, F., Zhang, G.J., 2018. ExoAPP: exosome-oriented, aptamer nanoprobe-enabled surface proteins profiling and detection. Anal. Chem. 90 (24), 14402–14411.
Kalluri, R., LeBleu, V.S., 2020. The biology, function, and biomedical applications of exosomes. Science 367, 641–656.
Kim, A., Bernt, W., Cho, N.J., 2019. Improved size determination by nanoparticle tracking analysis: influence of recognition radius. Anal. Chem. 91 (15), 9508–9515.
Kim, Y.S., Raston, N.H.A., Gu, M.B., 2016. Aptamer-based nanobiosensors. Biosens. Bioelectron. 76, 2–19.
Kowal, J., Arras, G., Colombo, M., Jouve, M., Morath, J.P., Primdal-Bengtson, B., Dingli, F., Loew, D., Tkach, M., Thery, C., 2016. Proteomic comparison defines novel markers to characterize heterogeneous populations of extracellular vesicle subtypes. Proc. Natl. Acad. Sci. U.S.A. 113 (8), E968–E977.
Li, P., Kaslan, M., Lee, S.H., Yao, J., Gao, Z., 2017. Progress in exosome isolation techniques. Theranostics 7 (3), 789–804.
Liu, C., Zhao, J., Tian, F., Cai, L., Zhang, W., Feng, Q., Chang, J., Wan, F., Yang, Y., Dai, B., Cong, Y., Ding, B., Sun, J., Tan, W., 2019. Low-cost thermophoretic profiling of extracellular-vesicle surface proteins for the early detection and classification of cancers. Nat. Biomed. Eng. 3 (3), 183–193.
Ma, H.T., Liu, J.P., Ali, M.M., Mahmood, M.A.I., Labanieh, L., Lu, M.R., Iqbal, S.M., Zhang, Q., Zhao, W.A., Wan, Y., 2015. Nucleic acid aptamers in cancer research, diagnosis and therapy. Chem. Soc. Rev. 44 (5), 1240–1256.
Mathieu, M., Martin-Jaular, L., Lavieu, G., Thery, C., 2019. Specificities of secretion and uptake of exosomes and other extracellular vesicles for cell-to-cell communication. Nat. Cell Biol. 21 (1), 9–17.
Meng, H.M., Liu, H., Kuai, H.L., Peng, R.Z., Mo, L.T., Zhang, X.B., 2016. Aptamer-integrated DNA nanostructures for biosensing, bioimaging and cancer therapy. Chem. Soc. Rev. 45 (9), 2583–2602.
Momen-Heravi, F., Getting, S.J., Moschos, S.A., 2018. Extracellular vesicles and their nucleic acids for biomarker discovery. Pharmacol. Therapeut. 192, 170–187.
Nair, S., Tang, K.D., Kenny, L., Punyadeera, C., 2018. Salivary exosomes as potential biomarkers in cancer. Oral Oncol. 84, 31–40.
Shao, H., Im, H., Castro, C.M., Breakefield, X., Weissleder, R., Lee, H., 2018. New technologies for analysis of extracellular vesicles. Chem. Rev. 118 (4), 1917–1950.
Sharma, S., Gillespie, B.M., Palanisamy, V., Gimzewski, J.K., 2011. Quantitative nanostructural and single-molecule force spectroscopy biomolecular analysis of human-saliva-derived exosomes. Langmuir 27 (23), 14394–14400.
Smith, P.K., Krohn, R.I., Hermanson, G.T., Mallia, A.K., Gartner, F.H., Provenzano, M.D., Fujimoto, E.K., Goeke, N.M., Olson, B.J., Klenk, D.C., 1985. Measurement of protein using bicinchoninic acid. Anal. Biochem. 150 (1), 76–85.
Tian, Y., Gong, M., Hu, Y., Liu, H., Zhang, W., Zhang, M., Hu, X., Aubert, D., Zhu, S., Wu, L., Yan, X., 2020. Quality and efficiency assessment of six extracellular vesicle isolation methods by nano-flow cytometry. J. Extracell. Vesicles 9 (1), 1697028.
van Niel, G., D'Angelo, G., Raposo, G., 2018. Shedding light on the cell biology of extracellular vesicles. Nat. Rev. Mol. Cell Biol. 19 (4), 213–228.
Wang, S., Zhang, L., Wan, S., Cansiz, S., Cui, C., Liu, Y., Cai, R., Hong, C., Teng, I.T., Shi, M., Wu, Y., Dong, Y., Tan, W., 2017. Aptasensor with expanded nucleotide using DNA nanotetrahedra for electrochemical detection of cancerous exosomes. ACS Nano 11 (4), 3943–3949.
Wang, T., Chen, C.Y., Larcher, L.M., Barrero, R.A., Veedu, R.N., 2019. Three decades of nucleic acid aptamer technologies: lessons learned, progress and opportunities on aptamer development. Biotechnol. Adv. 37 (1), 28–50.
Wang, Z., Zong, S., Wang, Y., Li, N., Li, L., Lu, J., Wang, Z., Chen, B., Cui, Y., 2018. Screening and multiple detection of cancer exosomes using an SERS-based method. Nanoscale 10 (19), 9053–9062.
Wu, L., Wang, Y., Zhu, L., Liu, Y., Wang, T., Liu, D., Song, Y., Yang, C., 2020. Aptamer-based liquid biopsy. ACS Appl. Bio. Mater. 3 (5), 2743–2764.
Xia, Y., Liu, M., Wang, L., Yan, A., He, W., Chen, M., Lan, J., Xu, J., Guan, L., Chen, J., 2017. A visible and colorimetric aptasensor based on DNA-capped single-walled carbon nanotubes for detection of exosomes. Biosens. Bioelectron. 92, 8–15.
Xing, X., Han, S., Li, Z., Li, Z., 2020. Emerging role of exosomes in craniofacial and dental applications. Theranostics 10 (19), 8648–8664.
Xu, R., Greening, D.W., Zhu, H.J., Takahashi, N., Simpson, R.J., 2016. Extracellular vesicle isolation and characterization: toward clinical application. J. Clin. Invest. 126 (4), 1152–1162.
Zhang, H., Wang, Z., Zhang, Q., Wang, F., Liu, Y., 2019a. Ti_3C_2 MXenes nanosheets catalyzed highly efficient electrogenerated chemiluminescence biosensor for the detection of exosomes. Biosens. Bioelectron. 124, 184–190.
Zhang, L., Xia, L., Xie, H., Zhang, Z., Pang, D., 2019b. Quantum dot based biotracking and biodetection. Anal. Chem. 91 (1), 532–547.
Zhang, X., Liu, C., Pei, Y., Song, W., Zhang, S., 2019c. Preparation of a novel Raman probe and its application in the detection of circulating tumor cells and exosomes. ACS Appl. Mater. Interfaces 11 (32), 28671–28680.
Zhang, Y., Wang, D., Yue, S., Lu, Y., Yang, C., Fang, J., Xu, Z., 2019d. Sensitive multicolor visual detection of exosomes via dual signal amplification strategy of enzyme-catalyzed metallization of Au nanorods and hybridization chain reaction. ACS Sens. 4 (12), 3210–3218.
Zhang, Z., Tang, C., Zhao, L., Xu, L., Zhou, W., Dong, Z., Yang, Y., Xie, Q., Fang, X., 2019e. Aptamer-based fluorescence polarization assay for separation-free exosome quantification. Nanoscale 11 (20), 10106–10113.
Zhong, W.Q., Ren, J.G., Xiong, X.P., Man, Q.W., Zhang, W., Gao, L., Li, C., Liu, B., Sun, Z. J., Jia, J., Zhang, W.F., Zhao, Y.F., Chen, G., 2019. Increased salivary microvesicles are associated with the prognosis of patients with oral squamous cell carcinoma. J. Cell Mol. Med. 23 (6), 4054–4062.
Zhu, C., Li, L.S., Wang, Z.J., Irfan, M., Qu, F., 2020a. Recent advances of aptasensors for exosomes detection. Biosens. Bioelectron. 160, 112213.
Zhu, F., Li, D., Ding, Q.F., Lei, C., Ren, L.Z., Ding, X.G., Sun, X.C., 2020b. 2D magnetic MoS_2-Fe_3O_4 hybrid nanostructures for ultrasensitive exosome detection in GMR sensor. Biosens. Bioelectron. 147, 111787.
Zlotogorski-Hurvitz, A., Dayan, D., Chaushu, G., Salo, T., Vered, M., 2016. Morphological and molecular features of oral fluid-derived exosomes: oral cancer patients versus healthy individuals. J. Canc. Res. Clin. Oncol. 142 (1), 101–110.